

Document downloaded from:

<http://hdl.handle.net/10251/197440>

This paper must be cited as:

Desantes, J.; Novella Rosa, R.; Pla Moreno, B.; López-Juárez, M. (2022). Effect of dynamic and operational restrictions in the energy management strategy on fuel cell range extender electric vehicle performance and durability in driving conditions. *Energy Conversion and Management*. 266:1-14. <https://doi.org/10.1016/j.enconman.2022.115821>



The final publication is available at

<https://doi.org/10.1016/j.enconman.2022.115821>

Copyright Elsevier

Additional Information

Highlights

Effect of dynamic and operational restrictions in the energy management strategy on fuel cell range extender electric vehicle performance and durability in driving conditions

J.M. Desantes, R. Novella, B. Pla, M. Lopez-Juarez

- FCREx dynamic and operation limits effect on performance and durability was evaluated
- Performance and durability change for FCREx vehicles in driving cycle was correlated
- Maximum durability (+110%) was achieved with $|di/dt|_{\max}=0.01 \text{ A/cm}^2\text{s}$, $i_{\min}=0.15 \text{ A/cm}^2$
- $|di/dt|_{\max}=0.001 \text{ A/cm}^2\text{s}$ or $i_{\min}=0.2 \text{ A/cm}^2$ do not allow charge-sustained operation
- Recommendations for FCREx vehicle and FC stack manufacturers were elaborated

Effect of dynamic and operational restrictions in the energy management strategy on fuel cell range extender electric vehicle performance and durability in driving conditions

J.M. Desantes, R. Novella*, B. Pla, M. Lopez-Juarez

*CMT-Motores Térmicos, Universitat Politècnica de València
Camino de vera s/n, 46022 Valencia (Spain)*

Abstract

Aiming at increasing fuel cell (FC) stack durability in driving conditions, part of the scientific community has focused its efforts on developing energy management strategies (EMS) for fuel cell hybrid vehicles (FCV). Nonetheless, most of these studies do not explicitly explain the effect of constraining the EMS in both degradation and performance when acting on the FC system dynamics or operational space nor consider the FC range-extender (FCREx) architecture for passenger car application. This study evaluates the potential of FCREx architecture to maximize FC stack durability and performance through control strategy dynamic and operational space limitations. For that purpose, a FCV modeling platform was developed and integrated together with an EMS optimizer algorithm and a semi-empirical advanced FC stack degradation model for driving cycle conditions. The resulting modeling platform was then simulated in WLTC 3b driving cycle to predict FC degradation and H₂ consumption with different dynamic and operational restrictions. Practical limits for EMS constraining were identified as $|di/dt|_{\max}=0.001$ A/cm²s or $i_{\min}=0.2$ A/cm² since they prevented the EMS from fulfilling the constant state-of-charge constraint in high-dynamic driving condition. In this sense, $|di/dt|_{\max}=0.01$ A/cm²s and $i_{\min}=0.15$ A/cm² were recommended as the combination of constraints that maximizes FC stack durability (+110%) without affecting the FCV operability with only an increase in of 4.7% in H₂ consumption. From these results, a set of recommendations and guidelines for FCREx vehicle manufacturers and FC stack developers were elaborated based on the benefits of understanding the dynamics and operational constraints that the FC system is going to be subjected to under real operation.

Keywords: Hydrogen, Proton Exchange Membrane Fuel Cell, Range Extender, Durability, Fuel cell hybrid electric vehicle, Driving cycle

1. Introduction

The use of hydrogen and fuel cell (FC) technology in the automotive sector has become one of the key solutions in the roadmaps aiming for industry decarbonization and the decrease in greenhouse gas (GHG) emissions [1, 2]. The existence of commercial fuel cell vehicles (FCV) proves that the integration of FC systems in passenger car applications is, nowadays, at the highest technological readiness level and complies with all the safety requirements for automotive applications. Nonetheless, the powertrain architecture for commercial passenger cars comprises a high-power FC stack

and a small-capacity battery [3]. This conventional FCV architecture has been widely studied in the literature together with variation integrating supercapacitors to optimize its operation to minimize consumption [4]. This sizing of the powertrain makes the FC stack operate under high-dynamic conditions since the battery is mostly used to complement the FC operation when extremely high dynamics or power over the FC system capabilities are required [5]. The dynamic behavior of FC systems for this application decreases significantly the durability of FC stacks, hence posing one of the main limitations for FC technology long-term mass-deployment in the automotive sector [6]. In order to allow slower dynamics in the FC system and improve the real range of FCV, given the limited number of hydrogen refueling stations worldwide [7], fuel cell range-extender (FCREx), also

*Corresponding author:

Email address: rinoro@mot.upv.es (R. Novella)

URL: www.cmt.upv.es (R. Novella)

called plug-in FCV architecture, was proposed for passenger car application. A recent study carried out by the authors has shown how this architecture, integrating a medium to high power FC system and a moderate-capacity battery, could improve the overall H_2 and energy consumption by 6.8% and 25% respectively compared to commercial FCVs [8] while decreasing significantly the cradle-to-grave GHG and NO_x emissions [9]. The results from these studies showed how the FCV architecture could be further improved to maximize the integration of FC technology in the automotive sector due to the increased flexibility and performance it offers. Nevertheless, currently, there is not any study that quantifies the potential improvement in FC stack durability that this specific architecture offers for passenger car applications. The enhancement in durability can be achieved by imposing severe limitations in the dynamics or in the operation space of the FC system since, different from conventional FCVs, the higher battery capacity allows for more intense use of it while fulfilling the charge sustaining condition. In this line, this study aims at identifying trends and quantifying the increase in durability and penalty in H_2 consumption when imposing operational restrictions on the energy management strategy (EMS) of the powertrain.

Most of the studies in recent years aimed at improving FC durability or performance for conventional FCV architectures [10], with low-capacity batteries, running with low-temperature FC, although some studies have been oriented towards high-temperature FC [11]. On the side of performance, some authors tried to improve the performance of FCVs, by making the EMS aware of the FC's state-of-health [12], or the durability, by integrating degradation models [13]. Nonetheless, among the latter studies, most of them based their degradation models on the semi-empirical constant degradation rates model developed by Pei et al. [14]. This model is a simplified version of the one used in this paper since it did not include either the effect of the operating conditions, in terms of temperature and relative humidity, or the intensity of the dynamics of the system in the degradation rates change. Given the simplicity of the model, it has been extensively used to predict FC stack durability and integrate it into EMS optimizer for FCV, be it alone [15] or together with battery degradation models [16]. The main advantage of this model is the fast calculation of the performance degradation that permits the realization of advanced techno-economic studies including the effect of FC degradation, such as that performed by He et al. [17]. However, the issue of using this model is that it is unaware of the changes in the operating conditions of the FC system when the dynamics are changed since it

quantifies load-change degradation as a constant degradation rate times the number of load-change cycles, independently of the oscillation frequency or the effect it has on the stack temperature and cathode/anode relative humidity. Furthermore, it is not useful to quantify the effect of limiting the operational space of the FC system since it has significant implications in the electrochemical waste heat, hence in the FC stack temperature which increases the membrane and catalysts degradation mechanisms.

Other authors such as Wang et al. [18] used the constant degradation rates model to build up other semi-empirical degradation models based on how the ECSA degrades according to the experimental degradation rates. The hypothesis behind this model is mainly that all the degradation is due to the catalyst layer degradation, thus neglecting the effect of membrane degradation over the voltage loss. This model was later used [19] to explore the use of rule-based energy management strategies to minimize the lifetime cost of the system integrating the battery degradation or traffic information, which implies low dynamics of the FCS.

The strategy that is mostly used to minimize FC degradation is to limit the dynamics of the FC system in such a way that load-change degradation, which is responsible for the highest decrease in durability, is minimized. For instance, in the study performed by Zhou et al. [20], in which degradation was controlled by including a term in the cost function, to be minimized by the energy management strategy optimizer, which quantifies the load-change rate of the FC system. As a consequence, they achieved a decrease of over 87% of FC system transients but, despite being regarded as positive, it was not clear how much impact it had on the durability. As such, other alternative strategies such as limiting the operational space of the FC system and the dynamics simultaneously may remain unexplored. In this sense, other studies focused on limiting degradation without quantifying it, just by imposing dynamic limitations during operating conditions at which high load may be requested to the FCS such as uphill driving conditions [21].

Although limiting the dynamics has been determined as one of the most promising control strategies to minimize FC degradation, other studies such as that proposed by Xing et al. [22] aimed to decrease the overall FC temperature to mitigate degradation. With that purpose, they achieved to stabilize the FC stack temperature to 350 K during driving conditions, which may be even higher under normal high-power conditions.

Alternatively, there are other semi-empirical degradation models in the literature based on other experimen-

tal data but they do not often include the effect of the FC stack temperature and relative humidity on degradation and performance [23]. In this line, it is possible to find in the literature studies such as that performed by Ma et al. [24], whose degradation model was developed by using a recurrent neural network with grid long-short term memory to predict the current modification due to degradation or that performed by Ou et al. [25], in which they modeled the degradation rate through a time-dependent exponential function acting on the exchange current density value. Other approaches such as that proposed by Raeesi et al. [26] are based on applying machine learning algorithms to fit empirical degradation models but they do not often include the sensitivity of FC degradation to the FC stack operating conditions.

Among the studies that considered FCREx architecture as an interesting architecture to minimize H₂ consumption [27], Zhang et al. [28] tried to maximize FC durability in a plug-in FCV by decreasing the active time of each stack and minimizing the switch-off and switch-on cycles but they did not include any degradation model and quantified degradation by considering that the operation time of each stack was proportional to their degradation rate, independently on how the FC stack was operated. In contrast, Martel et al. [29] considered this architecture and tried to optimize FC durability with the constant degradation rate model, thus ignoring the effect of temperature and relative humidity in enhancing the degradation mechanisms [30]. This shows how there is a knowledge gap with respect to the analysis of the potential of FC stack durability increase in FCREx vehicles. In this sense, performing sensitivity analyses is mandatory to understand the effect on performance and degradation rate of optimizing and restricting the energy management strategies when the FC system is integrated together with a battery with enough capacity in such a way that the powertrain power production does not have to rely mainly on the FC system. For that reason, this study aims at quantifying the effect of imposing limitations in the dynamics and in the operation space of a FC system integrated into a FCREx or plug-in FCV architecture on H₂ consumption and durability. In this sense, the main challenge faced in this study to accomplish such an objective was to develop a FCV vehicle with FCREx architecture modeling platform integrating not only all the subsystems required for normal driving cycle simulation but also a real-time EMS optimizer that can work in parallel and in real-time with a semi-empirical model suitable for driving cycle conditions, thus being aware of the degradation state of the FC stack and adapting the EMS to the FC state-of-health. Derived from this challenge, the combi-

nation of the models should be fast enough to run driving cycle simulations and the EMS must ensure that, given any combination of operational and dynamic restrictions, the H₂ consumption is mathematically minimized so that it is not possible to obtain a better solution with a given vehicle architecture and control strategy combination. This last item is particularly critical since in this study different control strategies are assessed and compared, so they must offer the highest propulsion system efficiency for the given constraints in the dynamics and in the operation to be comparable and avoid any bias coming from inaccuracies in the power split optimization.

1.1. Knowledge gaps

Considering the previous studies, the following conclusions can be extracted to provide an idea of the knowledge gaps in the literature about degradation prediction and optimization for FCREx vehicles:

1. FC stack durability increase potential has not been quantified for FCREx vehicles since most of the studies are applied over conventional FCVs (high-power FC stacks and low-capacity batteries).
2. The increase in FC stack durability when optimizing the control strategy has not been correlated to the consequent penalty in H₂ consumption for FCREx vehicles.
3. Most of the studies focus the strategy to maximize durability on limiting the dynamics of the FC system but, even in the cases in which degradation rate change is quantified, none considers the possibility of restricting part of the FC system operation or its combination with limited FC dynamics.
4. A significant part of the studies aiming at minimizing degradation rate through the energy management strategy optimization use constant degradation rates models that do not take into account either the effect of the load-change rate or the degradation mechanisms enhancement due to excessive temperature or relative humidity. This is critical to provide a good estimation for FC stack durability in driving conditions when the powertrain is subjected to sudden changes in its operating conditions.
5. There are no guidelines in the literature about how the control strategy for FCREx vehicles should be designed and constrained when aiming for both performance and durability optimization.

From the previous considerations, it is evident how the effect on durability and performance of FC systems

when imposing restrictions over the dynamics and the operation space has not been evaluated yet for FCREx architectures. For that reason, this study aims at understanding the potential decrease in FC stack degradation of FCREx vehicles through control strategy modification in driving cycle conditions.

1.2. Contribution and objectives

The main motivation and contribution of this paper are to identify and quantify the changes in both performance and durability when imposing restrictions on the dynamic and the operational limits of the FCS in relevant driving conditions, thus providing guidelines to design energy management strategies for automotive application. Complementary to this contribution, the study is performed over a vehicle with FCREx architecture, whose use in the literature for automotive applications is limited. In this sense, the specific contributions of this paper are:

- Quantify the potential increase in FC stack durability when imposing progressive restrictions in the FC system dynamics and the consequent penalty in H_2 consumption in driving conditions (knowledge gaps 1, 2 and 4).
- Quantify the change in FC stack durability and performance when imposing progressive restrictions in the FC system operational space by limiting the minimum current density in driving conditions (knowledge gaps 1, 2, 3 and 4).
- Identify practical limits for energy management strategy restrictions for FC systems powering FCREx vehicles (knowledge gaps 1 and 5).
- Understand how these restrictions affect each other and identify any potential cross-effect (knowledge gaps 1, 2 and 4).
- Elaborate recommendations for FCREx vehicle manufacturers about how the control strategy should be designed to maximize performance and durability and generate information to FC stack developers to help identify the degradation rate source relative relevance depending on the target control strategy (knowledge gap 6).

2. Methodology

In this section, the methodology followed to obtain the results of this study and the required simulation

tools are explained. As commented before, the idea behind this study is to understand the effect on both consumption and degradation in a FCREx vehicle, i.e., in an FCV with a high-capacity battery and a FC operating as a range-extender. For that purpose, a 60 kW FC stack and a 30 kWh battery FCREx design were selected and modeled from experimental results following the methodology described in previous studies [8].

To accomplish the main and the secondary objectives defined in section 1.2 the methodology followed is that presented in figure 1. First, the FCV modeling platform was developed integrating a validated FC stack model, a BoP which management was optimized to maximize FC system efficiency and other components describing the electrical and mechanical behavior of the vehicle, the battery and the e-motor (section 2.1). In order to quantify FC stack degradation, a semi-empirical degradation model for PEMFC technology was then developed to be working in parallel together with the vehicle model in driving cycle simulations (section 2.2). Then, a real-time degradation-aware EMS including the option to limit the FCS operational space and dynamics was integrated into the modeling platform (section 2.3). Finally, the modeling platform was used to simulate WLTC 3b driving cycle by imposing the dynamic and operational limitations defined in section 2.4, thus resulting in the discussion of the results in sections 3, 4 and 5.

The FCREx vehicle model, whose FC model was validated with experimental data, was simulated using the WLTC 3b driving cycle. This driving cycle is representative of the low, medium, high, and ultra-high dynamics driving. For that reason, apart from being the correspondent WLTP driving cycle for the selected vehicle given its power-to-mass ratio, this cycle was selected to understand the effect on both FC degradation and H_2 consumption when imposing restrictions on the EMS.

2.1. Fuel cell vehicle model

As stated previously, the FCREx model namely consists of a FC system whose stack maximum power is 60 kW, a battery with 30 kWh of energy capacity and a 5 kg H_2 tank. The vehicle body is that of a SUV-type to ensure that all the systems fit inside it, based on Hyundai Nexo FCV. The vehicle model, together with all the subsystems except for the EMS optimizer, was developed in GT-Suite v2020 software and validated with experimental data. GT-Suite is a modeling platform that is extensively used in the automotive industry for thermal fluid-dynamics simulation. In this software, the physics are solved by mainly applying the mass, species, momentum and energy conservation equations together with

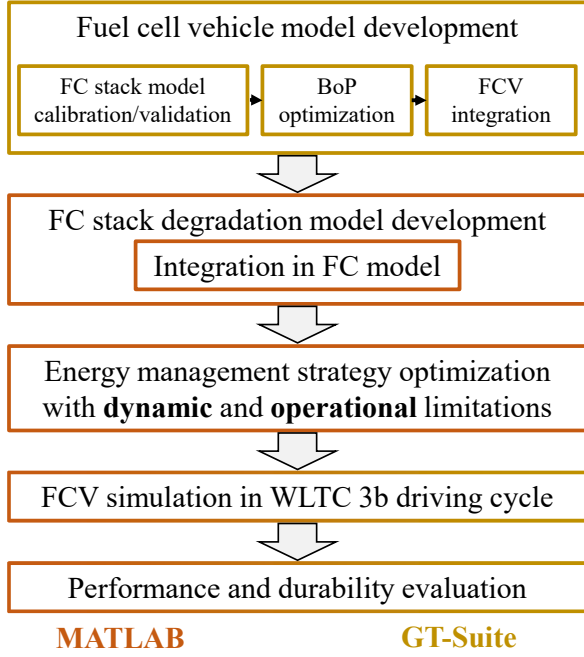


Figure 1: Outline of the methodology followed in this study.

well-known correlations and models based on experimental data. From v2020, GT-Suite also includes a FC model whose polarization curve depends on well-established correlations and conservation equations to describe the physics and electrochemistry of FC. This model has been previously used by the authors and described extensively in a previous study [8]. In this section, the model will be explained to provide the reader with enough information as to what are the main phenomena modeled in the FC stack, but for further detail, the reader should refer to a previous study [8].

The FC stack model was calibrated to experimental results so that its polarization curve reproduces the physical behavior of a reference stack. The polarization curve of the FC stack model is defined as:

$$V_{FC} = V_{OC} - V_{act} - V_{ohm} - V_{conc} \quad (1)$$

$$V_{act} = \begin{cases} \frac{R_{gas}T}{2F} \left(\frac{i}{i_0} \right) \\ \frac{R_{gas}T}{2\alpha F} \ln \left(\frac{i}{i_0} \right) \end{cases} \quad (2)$$

$$V_{ohm} = R I \quad (3)$$

$$V_{mt} = -C \ln \left(1 - \frac{i}{i_l} \right) \quad (4)$$

Where V_{OC} is the open-circuit voltage and V_{act} , V_{ohm} and V_{mt} are the activation, ohmic and mass transport losses, respectively. Advanced losses modeling was

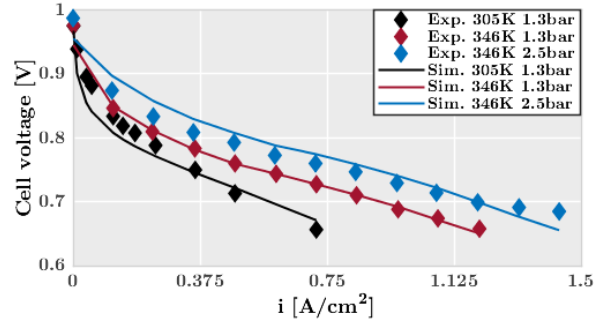


Figure 2: FC model validation results at different temperatures and pressures. Experimental data retrieved from [33, 34].

used to include the sensitivity of the ohmic resistance and the exchange current density to the FC operating conditions. Different from other studies in the literature, the polarization sensitivity of this model to temperature and pressure was calibrated so that it can capture the change in performance in driving cycle conditions when these conditions are under constant change. Following the study of Terada et al. [31], the ohmic resistance was modeled considering the water content along the membrane, which affects significantly its ionic conductivity from a reference ohmic resistance, thus modifying the heat losses as a consequence of the proton transport through it. The exchange current density was modeled so that it included dependency on the FC temperature, the oxygen partial pressure, the electrochemical activation energy, the electrode roughness and the reference exchange current density, as suggested by Murschenhofer et al. [32].

Considering this polarization curve modeling (equation 1), the reference ohmic resistance and exchange current density, the mass transport loss coefficient C , the charge transfer coefficient α and the open-circuit voltage were calibrated using a genetic algorithm optimizer matching simultaneously the polarization curve shape at different operating conditions of temperature and pressure with the experimental data in [33, 34]. Following this methodology, the FC stack model could reproduce the experimental data, as seen in figure 2, with an average error of 2%.

Once the FC stack model was validated, it was integrated into a BoP environment, conforming the FC system (figure 3). The balance of plant consisted of separated circuits for the different fluids used in the FC system. The cathode circuit (air path) was composed of an electric compressor, followed by a heat exchanger to decrease the temperature rise from the compressor pressure rise, and a humidifier that used the stack outlet wa-

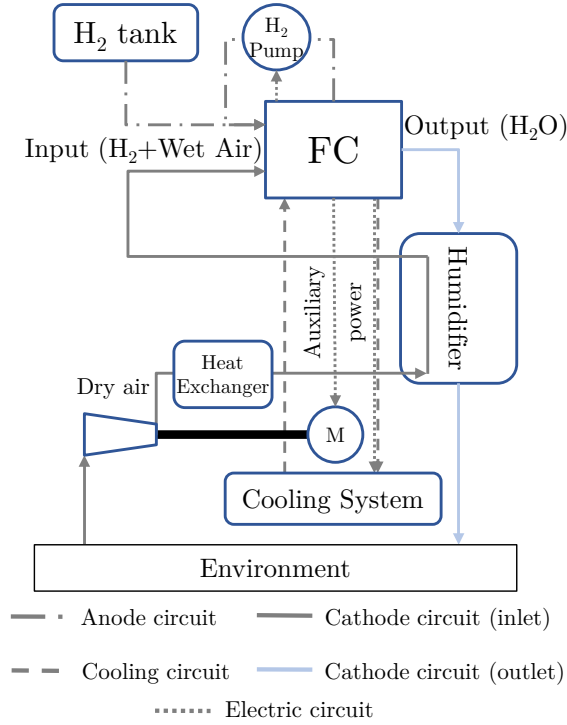


Figure 3: FC system sketch composed of the FC stack and the BoP components developed initially at [8].

ter vapor to humidify the cathode inlet. The control of the cathode was performed through the electric motor power and the exhaust air valve area control in such a way that cathode stoichiometry was no lower than 1.8 and the cathode pressure the one maximizing the FC system efficiency for the corresponding mass flow rate.

The anode circuit (H_2 path) is composed of the H_2 tank, a valve controlling the pressure difference between the tank and the stack, and an active H_2 recirculation loop, i.e., a pump controlling the mass flow recirculated from the anode outlet to the anode inlet to ensure enough anode stoichiometry for efficient and durable operation without starvation.

The coolant circuit followed the typical architecture of a cooler-air heat exchanger with a fan on the air side to enhance the heat transfer and control the coolant temperature along with a coolant pump to control the coolant mass flow rate through the stack depending on the actual and target temperature for the FC stack.

The management of the BoP was optimized to maximize the efficiency of the FC system defined as:

$$\eta_{FC_{sys.}} = \frac{P_{FC} - P_{BoP}}{P_{H_2}} \quad (5)$$

where $\eta_{FC_{sys.}}$ is the FC system efficiency, P_{FC} is the electrical power produced by the FC stack, P_{BoP} is the power consumed by the BoP, and P_{H_2} is the H_2 power consumed by the FC stack.

The optimization of the BoP management was performed in [8], achieving efficiencies over 60% without taking into account the DC-DC converter electric losses. The overall vehicle was optimized at two levels, the first level is the BoP management, while the second level is the energy management strategy governing the energy flow exchange between the different vehicle powertrain subsystems, described in section 2.3. With the data obtained from the BoP management optimization, the FC system was simplified to a mean values model to decrease the computational time. The temperature evolution in the simplified model was modeled through a thermal mass whose characteristics were adjusted through genetic algorithms to match the thermal response of the complex model in the WLTC 3b driving cycle with an RMS error of 1.2%.

The FC system was then integrated into an indirect FCV electronic architecture, characterized by the presence of separate DC-DC converters for the battery and the FC system, as well as an AC-DC converter (inverter) for the electric motor of 120 kW. This electronic configuration is nowadays used for modern FCVs since the DC-DC converter at the output of the FC system allows the downsizing of the FC stack, thus decreasing the powertrain weight, and protecting it from potential fluctuations coming from the DC-DC bus system.

2.2. Degradation model

Fuel cell degradation rate depends both on how it is operated (EMS) and on which conditions it is operated. On one hand, degradation sources may come from the different electrochemical mechanisms triggered at low-load or high-load conditions, as well as from natural degradation and load-change (high dynamics) conditions. These degradation mechanisms change depending on the voltage at which each cell is operated and the flow of protons through the membrane, which determines the rate of the main electrochemical processes inside the FC stack and is proportional to the current density. On the other hand, these phenomena are chemical by nature, so they depend on the operating temperature (T) and the water presence (RH) in both the cathode and the anode.

The presented degradation model takes into account all these phenomena from physical trends that are expressed as scaling functions applied over degradation rate coefficients obtained from reference conditions of known i , T and RH . The reference degradation rates

Control input (u)	Fuel cell power	P_{FC}
State	Energy in the battery	E_b
Objective/Cost function	H ₂ consumption minimization	$J = \int_{t_0}^{t_f} P_f(u(t), t) dt$ (6)
Constraint	Battery charge sustaining	$\int_{t_0}^{t_f} P_b(u(t), E_b(t), t) dt = 0$ (7)
Algorithm	Pontryagin's Minimum Principle (PMP)	

Table 1: Energy management's main characteristics

Condition	δ [fraction V loss]
Low power [h] $\left(\frac{d\delta}{dt}\right)_{lp,ref}$	$1.26 \cdot 10^{-5}$
Load change [cycle] $\left(\frac{d\delta}{dn_{lc}}\right)_{ref}$	$5.93 \cdot 10^{-7}$
High power [h] $\left(\frac{d\delta}{dt}\right)_{hp,ref}$	$1.03 \cdot 10^{-5}$
Start-stop [cycle] $\left(\frac{d\delta}{dn_{ss}}\right)_{ref}$	$1.96 \cdot 10^{-5}$

Table 2: Reference degradation rates (1st layer) to be scaled.

were obtained experimentally from [14] and further adjusted for model validation purposes (table 2). This model was developed and validated in previous studies. As such, it is explained in this study for completeness but for further information, the reader should refer to [35].

The degradation is expressed as a voltage degraded ratio $\delta = 1 - V_{deg}/V_{FC}$ where V_{FC} and V_{deg} are the non-degraded and degraded FC stack voltage, respectively. The model acts on the rate change of δ with time by modifying the reference degradation rates (table 2) depending on the electrochemical phenomena and the operating conditions as:

$$\delta = \int_0^t \left[\frac{d\delta}{dt}\Big|_{lp} + \frac{d\delta}{dt}\Big|_{lc} + \frac{d\delta}{dt}\Big|_{hp} + \frac{d\delta}{dt}\Big|_{nt} \right] dt + \frac{d\delta_{ss}}{dn_{ss}} n_{ss} \quad (8)$$

$$\frac{d\delta}{dt}\Big|_{lp} = \frac{d\delta}{dt}\Big|_{lp,ref} \cdot \xi_{lp}(i) \cdot \tau(T) \cdot \eta(\overline{RH}) \quad (9)$$

$$\frac{d\delta}{dt}\Big|_{lc} = \frac{d\delta}{dn_{lc}}\Big|_{ref} \cdot \xi_{lc}\left(\frac{di}{dt}\right) \cdot \tau(T) \cdot \eta(\overline{RH}) \quad (10)$$

$$\frac{d\delta}{dt}\Big|_{hp} = \frac{d\delta}{dt}\Big|_{hp,ref} \cdot \xi_{hp}(i) \cdot \tau(T) \cdot \eta(\overline{RH}) \quad (11)$$

$$\begin{aligned} \frac{d\delta}{dt}\Big|_{nt} = & \frac{\frac{d\delta}{dt}\Big|_{hp,ref} \xi_{hp}(i_{hp}) - \frac{d\delta}{dt}\Big|_{lp,ref} \xi_{lp}(i_{lp})}{i_{hp} - i_{lp}} (i - i_{lp}) \\ & + \frac{d\delta}{dt}\Big|_{lp,ref} \xi_{lp}(i_{lp}) \end{aligned} \quad (12)$$

$$\frac{d\delta_{ss}}{dn_{ss}} = \frac{d\delta}{dn_{ss}}\Big|_{ref} \quad (13)$$

where ξ , τ and η are scaling functions used to increase or decrease the degradation rates depending on the current density (electrochemical phenomena), temperature and relative humidity (operating conditions) respectively. i_{hp} is the minimum current density at which high-power degradation is considered and i_{lp} is the maximum current density for which low-power degradation is considered. These parameters were calibrated to 1 and 0.33 A/cm² from experimental data [14].

ξ_{lp} scales the degradation rate with the intensity of the degradation mechanisms at low power conditions (commonly known as idle condition). The increase in the activity of these degradation mechanisms was obtained from experimental data showing the change in fluoride release rate (FRR) which indicates membrane degradation [36] and the catalyst surface carbon corrosion and its effect on anodic peak current [37], which indicates FC performance decay. This function is 1 at 0.01 A/cm², at which the reference degradation rates

were measured.

$$\xi_{lp}(i) = -0.176 \cdot \ln i + 0.169 \quad (14)$$

High-power degradation scales with H^+ flow through the membrane, i.e., with current density since at this condition the main effect over degradation comes from the higher heating of the FC stack, rather than from any mechanism that may activate at high power. However, it is expected that the degradation rate increases with the rate at which the electrochemical phenomena occur inside the FC. As such, ξ_{hp} can be defined as:

$$\xi_{hp} = \frac{i}{i_{hp}} \quad (15)$$

Load-change degradation scales with the current density change rate ($|di/dt|$). However, as the reference data was obtained for a given i oscillation with a known amplitude $|\Delta i|_{ref}$ and the model evaluates the degradation rate at each time step dt , it is necessary to scale degradation rate due to load-change conditions with the change in the current density for the given time step $|\Delta i|_{dt}$. As such, ξ_{lc} was defined as:

$$\xi_{lc} \left(\frac{di}{dt} \right) = \frac{|\Delta i|_{dt}}{2|\Delta i|_{ref}} \quad (16)$$

where 2 was added to the denominator to account for both the increase and decrease in current density in the reference voltage cycling test.

Natural or medium-power degradation was modeled considering the continuity of the degradation rates between the low-power and high-power conditions. Note that calling this degradation source *natural* does not mean that it is comprising all the natural degradation phenomena in the FC stack. It means that in the range in which this degradation rate and scaling functions are applied, steady-state degradation can only be attributed to natural decay since the most significant degradation mechanisms detected at low-power and high-power conditions are not present in this range of current densities.

The effect of the operating conditions on degradation rate was accounted for through the effect of T and RH in the FC stack. Including the effect of temperature is motivated by the chemical nature of degradation, which implies a strong dependency of the reaction rate on the thermal state of the reactants and products. The scaling function for the T was developed based on the experimental results in [36] showing the dependency of FRR

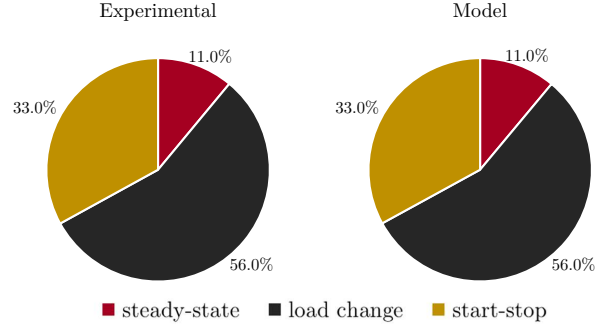


Figure 4: Degradation rate source validation with experimental results from [14]. Steady-state degradation comprises low-power, high-power and natural degradation.

on the operating temperature (membrane degradation) and in [38] showing the effect of T on electrochemical surface area (ECSA) decrease rate due to Pt surface loss through Pt dissolution mechanism:

$$\tau(T) = -5.390 \cdot 10^{-4} T^2 + 0.399 \cdot T - 71.576 \quad (17)$$

being it valid in the range of $T \in [310, 373.15]$ K.

The effect of RH on degradation is accounted for by taking RH as the average relative humidity between the anode and the cathode. Water excess (high RH) in the membrane electrode assembly increases the ECSA degradation rate through the Pt grain growth mechanism. η function scales the degradation rate with RH and was obtained based on the experimental results obtained from [39] where voltage cycling degradation tests were performed at different RH conditions:

$$\eta(RH) = 0.10646e^{0.028 \cdot RH [\%]} \quad (18)$$

The model was validated by simulating the real driving conditions of a FC stack for a city bus on a daily route [14] and comparing the experimental degradation results with those provided by the model. Degradation was predicted with an error lower than 0.1% (figure 4). The results in figure 4 are shown in relative terms for simplicity although they are equivalent in absolute terms since the start-stop cycling degradation for the model was directly obtained from the experimental results.

2.3. Energy management strategy

The optimum control of any powertrain composed of different power generation systems consists of finding

the power-split sequence that minimizes the cost function [40]. For benchmarking and fair comparison purposes, the usual strategy is to solve the optimal control (OC) problem for each design so that the results reflect the best-case control of the system, avoiding any potential bias towards any design. In the present study, the EMS is restricted in its dynamic behavior and operational limits to understand the implications of limiting it on H₂ consumption and durability. As such, each simulation should reflect the optimal control with a given restriction on the EMS so that the comparison is performed fairly.

The overall description of the EMS optimizer along with the definition of all the important parameters is compiled in table 1. The cost function J (eq. 6) represents the H₂ consumption along the driving cycle in energy terms, which is calculated by integrating over time the H₂ power consumed (P_f) controlled through the control variable u , which, for this study, is the FC stack current density i . When FCREx vehicles are operating with the FC as a range-extender, the battery is actuated in such a way that the state-of-charge (SOC) or energy contained (E_b) is sustained along the driving cycle. This condition is imposed as a constraint for the EMS optimizer (eq. 7) by setting the EMS target to keep the cumulative power consumed by the battery (P_b) to 0 along any driving condition.

The OC problem is solved by applying the Pontryagin's Minimum Principle (PMP). According to it, any OC problem can be solved by choosing the optimal solution at each time step, which will provide the optimal solution for the set of conditions along the problem's length. The PMP states the necessary conditions for optimal trajectories in the control and state of a dynamic system. PMP applied to the case at hand implies:

$$H(u^*, E_b^*, \lambda^*, t) \leq H(u, E_b^*, \lambda^*, t) \forall u \in U, t \in [t_0, t_f] \quad (19)$$

where u^* and E_b^* are the optimal trajectories of the control and state of the problem and H is the Hamiltonian function, defined as:

$$H = P_f - \lambda \dot{E}_b = P_f(u(t), t) + \lambda(t) P_b(u(t), E_b(t), t) \quad (20)$$

According to the PMP, the dimensionless co-state λ varies with the evolution of H respect to the state E_b :

$$\dot{\lambda} = \frac{\partial H}{\partial E_b} \quad (21)$$

Combining with eq. 20:

$$\dot{\lambda} = \lambda \frac{\partial P_b}{\partial E_b} = \lambda P_{batt} \frac{\partial (P_b/P_{batt})}{\partial E_b} \quad (22)$$

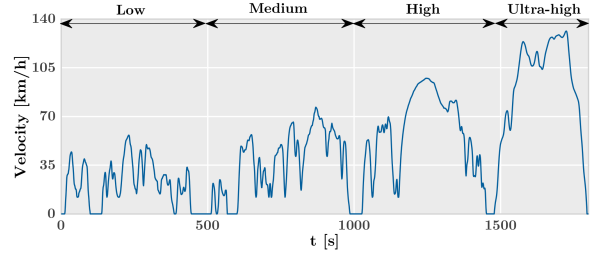


Figure 5: WLTC 3b driving cycle velocity profile.

P_b/P_{batt} the battery power consumed over the battery power produced, i.e., the inverse of the battery efficiency. When the battery state-of-charge is controlled around a fixed value, which is by definition the battery behavior in range-extender or charge-sustaining mode, the variation of the efficiency with its energy level E_b is small. Therefore, according to equation 22, the co-state λ can be assumed constant [41]. As a consequence, the OC problem is reduced to find iteratively the value of λ that fulfills the charge-sustaining condition (eq. 7). A more detailed description of the EMS optimization algorithm can be found in previous studies [8].

For the present study, the restrictions on $|di/dt|$ and i_{min} are imposed by means of step functions affecting the cost function J . In this sense, the Hamiltonian function, to be minimized each time step, is replaced by:

$$H = P_f - \lambda \dot{E}_b + L_1 + L_2 \quad (23)$$

where L_1 and L_2 are the limiting functions that increase the cost function value to infinite for the values of the control variable u (current density) out of the imposed bounds at each time step so that the EMS optimizer discards the operation at these points.

$$L_1 = \begin{cases} 0 & u \geq i_{min} \\ inf & u < i_{min} \end{cases} \quad (24)$$

$$L_2 = \begin{cases} 0 & |di/dt|(t+dt) \leq |di/dt|_{max} \\ inf & |di/dt|(t+dt) > |di/dt|_{max} \end{cases} \quad (25)$$

2.4. Sensitivity analysis description

Once the modeling platform integrating the FC vehicle model and submodels, the EMS optimizer and the FC stack degradation model were developed, a set of simulations considering the WLTC 3b cycle (figure 5) were carried out. These simulations were then used to generate figures 6-22 to understand the effect of the EMS restrictions on H₂ consumption, total FC degradation rate and FC degradation rate by source.

Dynamic limitation [A/cm ² s]	i_{\min} [A/cm ²]	0	0.1	0.15	0.2
Inf		X	X	X	X
0.1		X	X	X	X
0.05		X	X	X	X
0.01		X	X	X	X
0.005		X	X	X	X
0.001		X	X	X	X
0.0005		X	X	X	X

Table 3: Simulation matrix defining the EMS restrictions in terms of the dynamic limitation and the minimum current density for each simulation.

In order to achieve enough resolution in the results for the analysis, the inferior limit in terms of dynamic limitation was set to 0.001 A/cm²s and the upper limit for the minimum current density constraint was set to 0.2 A/cm² from preliminary simulations. Once the extreme restrictions were defined, the simulations defined in the simulation matrix (table 3) were carried out.

3. Effect of limiting $|di/dt|$

Limiting $|di/dt|$ during driving cycle operation has a direct impact on how the EMS optimizer controls the energy flows generated by the FC system. Taking into account that the boundary condition for the EMS is to keep the battery SOC at the same value at the beginning and at the end of the driving cycle (charge sustaining), any limitation on the EMS that does not allow the FC system to operate at the optimum condition needs to be compensated by increasing the power produced (current density) at other operating conditions. As such, imposing limitations on the FC system dynamics has an impact not only on those conditions that the FC system can not reach due to the EMS restrictions but also on the whole cycle. This implies that the current density evolution along the driving cycle is going to be significantly affected, not only in the high-dynamics region of the cycle. Figure 6 shows both the current density and the current density change rate along the simulated driving cycle. The evolution of the current density with time is very similar in the cases where $|di/dt|$ is not limited and where the limitation is 0.1 A/cm²s since high-dynamics is also possible with such limitation. Therefore, the intensity of the load-change oscillations and their ampli-

tude is similar in both cases. However, it is possible to detect some differences between these two control strategies. First, the current density peaks are higher until 1500 s for the non-limited case, meaning that to achieve that current density evolution, high dynamics are required. Therefore, at these peaks, the operation of the case with $|di/dt| \leq 0.1$ A/cm²s is suboptimum. To compensate for this deviation from the optimum operation the $|di/dt| \leq 0.1$ A/cm²s case needs to provide additional power from 1500 s, in the high-power demand part of the cycle, where the current density rises to 0.8 A/cm². Compared to these two cases, those with $|di/dt| \leq 0.01$ A/cm²s and $|di/dt| \leq 0.001$ A/cm²s present a smoother current density evolution. In these cases, the dynamics of the load-change (represented by $|di/dt|$) are clearly lower by imposition while the amplitude of such oscillations is lower in both cases. For both cases, it is possible to identify how the minimum current density along the cycle increases to compensate for the points where its operation is suboptimum. This behavior is accentuated the higher the restrictions on $|di/dt|$. Nonetheless, apart from slower dynamics, the case with $|di/dt| \leq 0.001$ A/cm²s also presents significantly lower load-change oscillations amplitude since the slow dynamics prevent the FC system from reaching high current densities. The limited variation in the absolute value of the FC current density suggests that the behavior of the FC system may be affected by the value of the current density at the beginning of the driving cycle.

The second graph in figure 6 shows how the dynamics of each case change with the limitations. This graph, besides from serving to verify that the $|di/dt|$ restrictions are correctly implemented, is useful to understand that for the modeled FCReX vehicle the $|di/dt|$ along the cycle without any restrictions on the EMS is mostly kept below 0.5 (reaching values around 1 occasionally). As such, soft limitations on $|di/dt|$ such as limiting it to 0.1 A/cm²s allow high dynamics and a FC system behavior close to the non-restricted case. This implies that to perceive significant changes in both degradation rates and H₂ consumption, $|di/dt|$ should be limited to values around 0.01 A/cm²s or lower.

The effect of modifying the current density evolution as in figure 6 on degradation can be perceived in the different degradation rate sources in figures 7-10. Even though it is expected that the major effect of limiting the dynamics of the FC system is identified in the load-change degradation rate, the resulting change in the current density evolution to compensate for the suboptimum operation affects other degradation sources such as low-power and natural (medium-power) degradation.

Regarding the low-power degradation source (figure

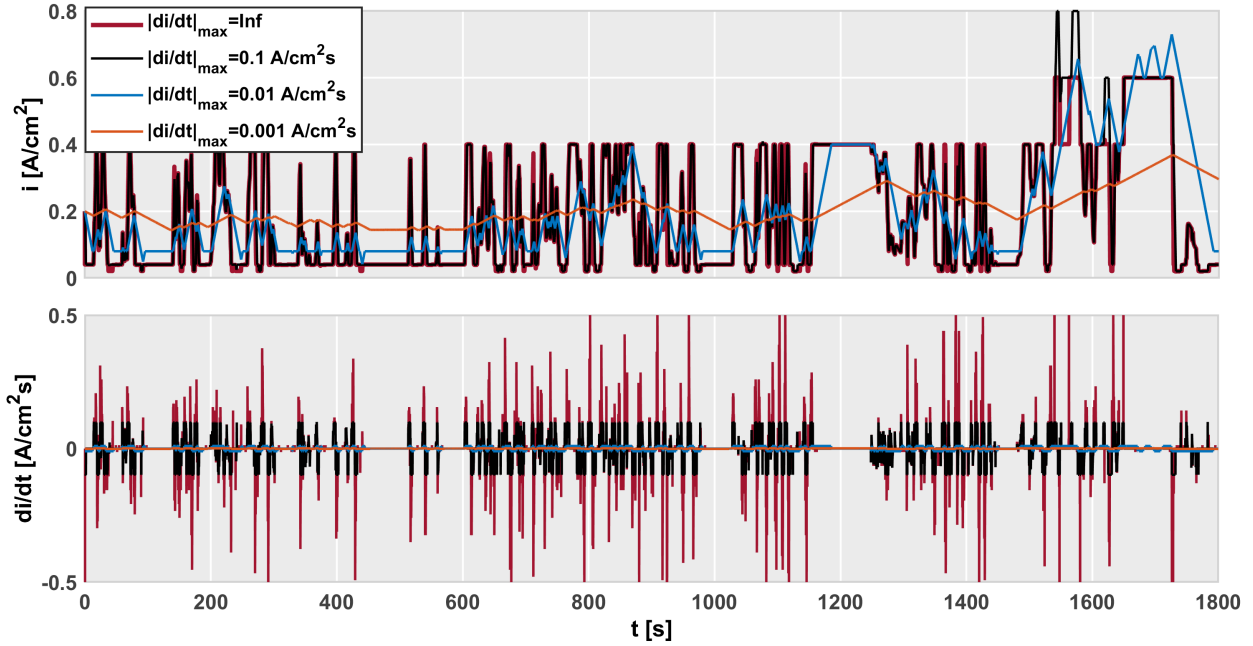


Figure 6: Current density and current density variation rate evolution along the WLTC 3b driving cycle with different restrictions on $|di/dt|$.

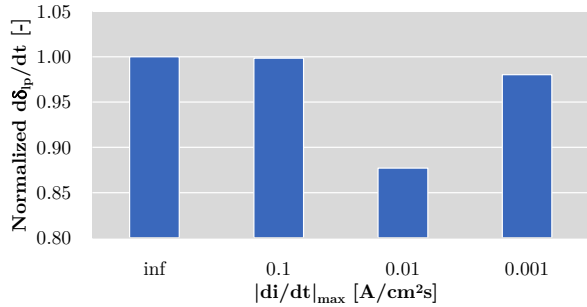


Figure 7: Normalized low-power degradation rate variation with $|di/dt|_{\max}$.

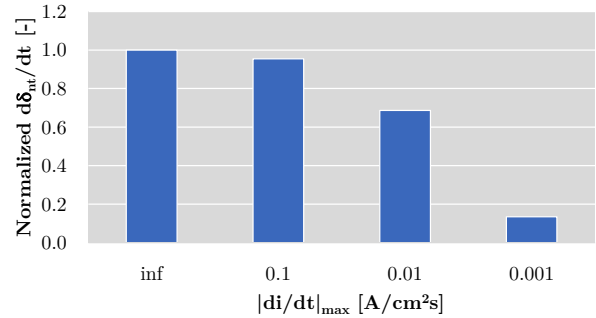


Figure 8: Normalized natural (medium-power) degradation rate variation with $|di/dt|_{\max}$.

7), following the change in the current density evolution when limiting $|di/dt|$, the cases with no dynamic limitation and $|di/dt| \geq 0.1 \text{ A/cm}^2\text{s}$ have the same behavior in the low-power current density region $i < 0.33 \text{ A/cm}^2$, which justifies values of the normalized degradation rate for these cases in figure 7. Increasing further the dynamic limitation to $0.01 \text{ A/cm}^2\text{s}$ increases the minimum current density, thus decreasing the degradation rate caused by electrochemical scaling as in equation 14. This implies a decrease in the degradation rate produced in steady-state low-power conditions. Nonetheless, if the dynamic limitation is even further increased to $0.001 \text{ A/cm}^2\text{s}$ the slow evolution of the FC current density does not allow achieving medium or high-power

conditions often so the FC stack operates mostly under low-power conditions. This fact, even though it may decrease the operating temperature of the stack (lower electrochemical losses) increases the degradation rate produced under low-power conditions.

Following the same reasoning as for low-power degradation, medium-power or natural degradation decrease the higher the dynamic limitation (figure 8) since the overall operating current density becomes lower, thus the FC stack is less time under the condition at which steady-state degradation can be attributed only to the natural decay of the catalyst and membrane properties.

As expected, load-change degradation is the most-

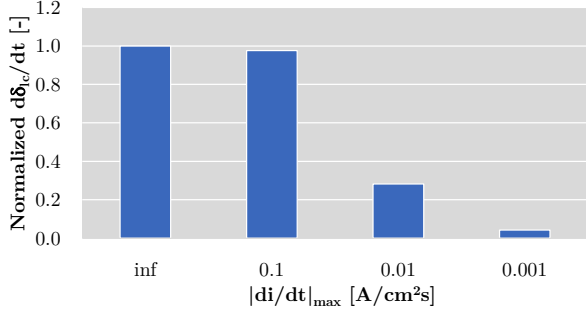


Figure 9: Normalized load-change degradation rate variation with $|di/dt|_{\max}$.

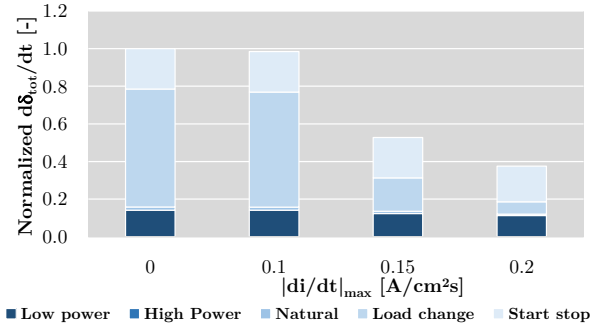


Figure 10: Normalized total degradation rate variation with $|di/dt|_{\max}$ segmented by source.

affected degradation rate source when limiting the dynamics due to both the decrease in the rate of change of the current density and in the amplitude of load-change oscillation.

The net effect of imposing dynamic limitations on FC stack durability can be seen in figure 10, on which the normalized total degradation rate variation is presented. As explained in figures 7-9, small dynamic limitations (0.1 A/cm²s) do not affect durability substantially while increasing them to 0.01 and 0.001 A/cm²s may decrease the total degradation rate by 47% and 62% respectively. This implies an increase in the FC stack lifetime of 89% and 166%. In accordance with most of the studies in the literature, load-change degradation is the major degradation source, hence decreasing it through dynamic limitations in the control strategy implies a significant increase in the stack durability. As can be seen in figure 10, load-change degradation is the most affected source.

Nonetheless, even though the degradation rate has decreased substantially when limiting the dynamics, imposing constraints on the control strategy whose sole objective is to decrease H₂ consumption has an impact on the overall vehicle efficiency. Figure 11 shows this impact in terms of H₂ consumption. The greater the

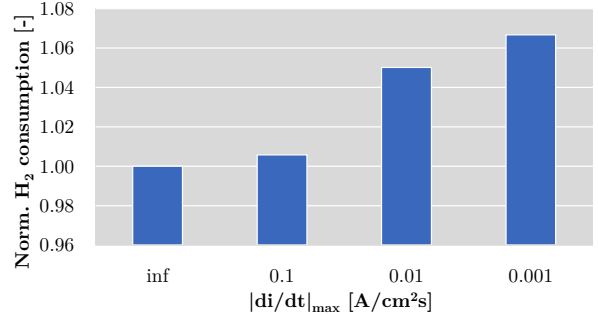


Figure 11: Normalized H₂ consumption variation with $|di/dt|_{\max}$.

dynamic limitation, the higher the penalty in H₂ consumption, achieving increments of 5% and 6.7% in the cases of 0.01 and 0.001 A/cm²s, respectively. This is indicative of how much of a trade-off is imposing dynamic limitations. For that reason, given the penalties in terms of H₂ consumption, the vehicle manufacturers that are considering the FCReX architecture should impose the dynamic limitation in the EMS that enables the FC stack of the designed vehicle to achieve the target life for a particular application and avoid constraining further the dynamics of the FC system to optimize H₂ consumption.

4. Effect of limiting i_{\min}

The other limitation on the EMS that has yet to be explored is to avoid the FC to operate under a certain value of current density, i.e., limiting the minimum current density (i_{\min}). This restriction is important and has a clear effect on degradation because it significantly affects the EMS optimizer behavior. As can be seen in the first graph of figure 12, the high dynamics are mostly preserved among the different simulated cases. Nonetheless, despite finding a high rate of change in the load-change oscillations (di/dt), it is clear that the load-change cycle amplitude decreases, meaning that there should be a significant effect on the main FC degradation source, i.e., load-change degradation. Furthermore, the suboptimum operation induced when imposing limitations on i_{\min} fosters on one hand, lower current density peaks and, on the other hand, less oscillations (see case with $i_{\min}=0.15$ A/cm² compared against cases with $i_{\min}=0.1$ A/cm² and $i_{\min}=0$ A/cm²). The lower and less frequent current density peaks are due to the fact that a significant amount of extra power is produced when the FC is trying to operate under low current densities but stays at the limited i_{\min} , hence the EMS does not require the FC to operate under high current densities

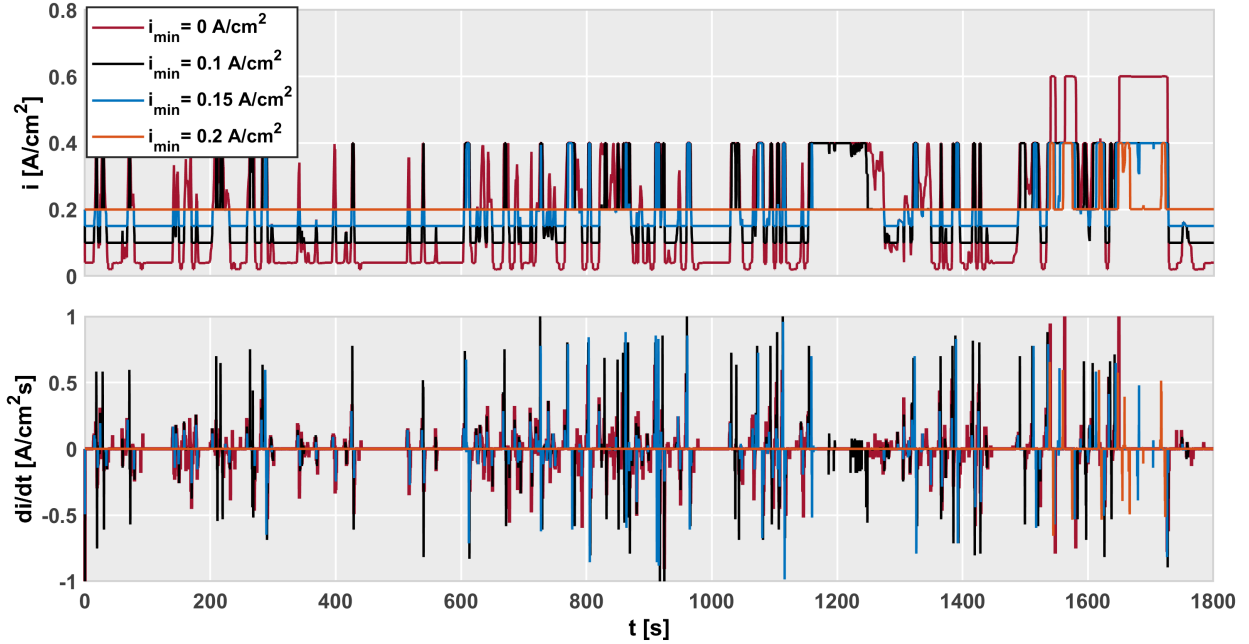


Figure 12: Current density and current density variation rate evolution along the WLTC 3b driving cycle with different restrictions on i_{\min} .

that often to fulfill the charge sustaining boundary condition. As is expected operating at higher current densities may decrease the FC degradation coming from the low-power (idle) degradation mechanisms that are more relevant the higher the FC voltage.

Despite perceiving the mentioned changes in the load-change oscillations and on the overall current density evolution along the driving cycle, high restrictions on i_{\min} are not recommended, although they may provide significant benefits in terms of durability. This is the case of limiting the i_{\min} to 0.2 A/cm^2 , where the FC operates at $i=i_{\min}$ during most of the cycle, except at the high-power region of the WLTC 3b cycle. Given this current density evolution, the charge sustaining condition might not be fulfilled with higher restrictions on i_{\min} or at different driving cycles where the brake power demand is lower. As such, imposing limits on the minimum current density must be done carefully, as it may affect significantly the operation mode of the FCReX vehicle, making it unfeasible for certain driving conditions.

The intensity of the load-change oscillations, represented in the second graph of figure 12 increases limiting i_{\min} compared to the non-restricted case at the high current density peaks to compensate for the suboptimum operation. Nonetheless, the non-restricted case presents more points where $di/dt \neq 0$ since the optimum operation that the EMS optimizer is imposing is that of

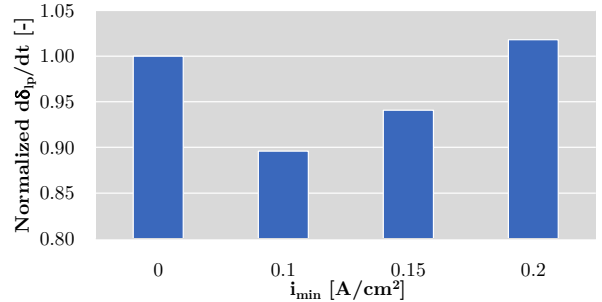


Figure 13: Normalized low-power degradation rate variation with i_{\min} .

the FC following, up to a certain extent, the electric motor power demand. In general, except for the case in which $i_{\min}=0.2 \text{ A/cm}^2$, it is difficult to extract a conclusion about what happens with the effect of load-change oscillations intensity over degradation just by looking at the current density evolution. However, an overall decrease in load-change degradation can be expected since a clear decrease in load-change oscillations amplitude is perceived.

Based on the change in the evolution of the current density and current density change rate (figure 12) it is possible to understand the variation of the different degradation rate sources. Low-power degradation (figure 13) presents two trends depending on the

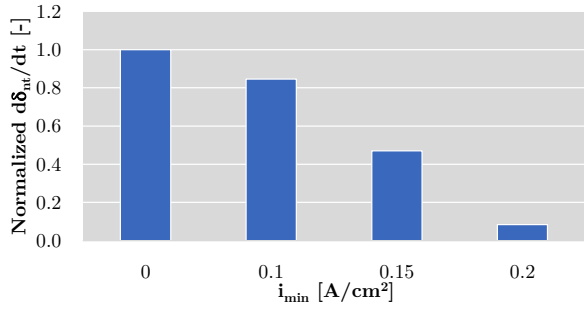


Figure 14: Normalized natural (medium-power) degradation rate variation with i_{\min} .

constraint. When comparing the non-limited and the $i_{\min}=0.1$ A/cm² cases it is possible to see a decrease in low-power degradation rate. This decrease is mainly due to the overall increase in the current density, which makes the FC stack operate under lower voltages, thus limiting the intensity of the degradation mechanisms that appear at low current density (equation 14). Nevertheless, when increasing further the limitation in the minimum current density, the low-power degradation grows. This fact, although it seems counterintuitive, is produced for two reasons. First, the overall increase in the current density implies higher electrochemical losses which, irretrievably, implies higher dissipated heat in the stack and the subsequent increase in the temperature of operation. The increase in the temperature enhances the degradation rate following equation 17. Second, following the charge sustaining condition imposed in the control strategy, increasing the minimum current density implies higher power production along the driving cycle, which prevents the FC stack from operating at medium or high current densities. In this case, this has as a consequence that the FC stack operates longer at <0.33 A/cm², thus increasing the time under which the FC stack suffers from low-power degradation.

Medium-power or natural degradation rate decreases the higher the i_{\min} (figure 14) since the overall increase in the current density in the low-power region implies that the FC stack no longer needs to reach medium or high-power current densities to fulfill the charge sustaining condition.

Although the dynamics of the stack are not limited when imposing constraints in i_{\min} , a significant decrease in load-change degradation is perceived in figure 15 the higher the lower limit for the current density. This is mainly due to the decrease in the amplitude of the load-change oscillations shown in figure 12. As explained before, imposing limitations in i_{\min} has a direct effect on the overall current density evolution, decreasing even

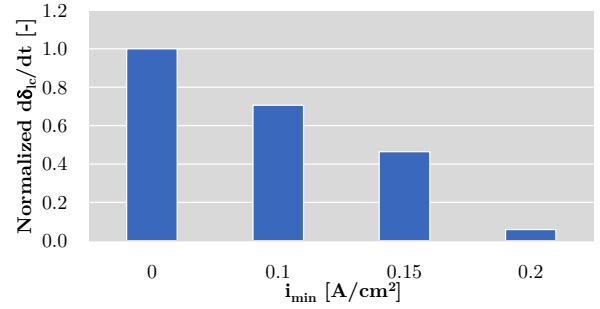


Figure 15: Normalized load-change degradation rate variation with i_{\min} .

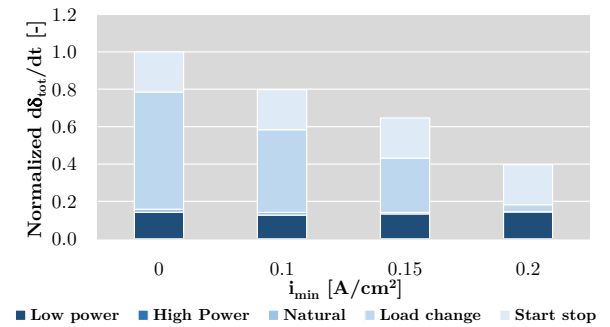


Figure 16: Normalized total degradation rate variation with i_{\min} .

its maximum value along the driving cycle. Furthermore, in the extreme case of limiting the minimum current density to a value of 0.2 A/cm², most of the load-change oscillations disappear since the additional power provided when the current density is 0.2 A/cm² makes the optimum FC stack behavior no longer follow the e-motor power demand to achieve constant battery state-of-charge. Nonetheless, after testing this restrictive condition in other driving cycles such as ARTEMIS Motorway, it was deemed too constricting since it may not allow fulfilling the charge sustaining condition in high-dynamics driving conditions.

The overall effect of limiting the minimum current density is a decrease in the total degradation rate (figure 16), namely motivated by the decrease in load-change degradation which compensates for the increase in low-power degradation. As such, depending on the constraint, the degradation rate may decrease by 21% with low limitation ($i_{\min}=0.1$ A/cm²) or by 60% when extreme restrictions are imposed (0.2 A/cm²).

Analogous to figure 11, figure 17 shows the increase in H₂ consumption when imposing limitations on the minimum current density. Note that imposing any limitation on i_{\min} implies narrowing the operation space of the FC system. Particularly, increasing the lower

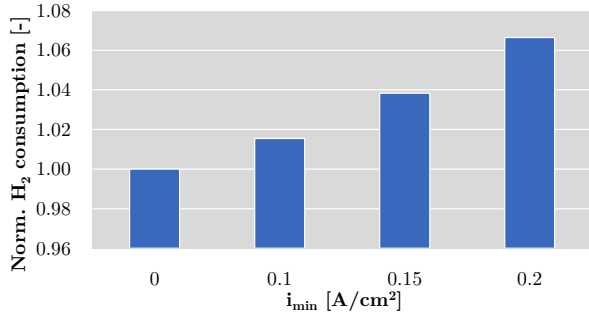


Figure 17: Normalized H₂ consumption variation with i_{\min} .

limit of the operation space for any power generation system means neglecting the option to minimize the fuel consumption locally, which in turn, has significant implications in terms of fuel consumption optimization penalty. For that reason, even the lowest limitation of the minimum current density considered in this study (0.1 A/cm²) has as a consequence a noticeable increase in H₂ consumption of 1.5%. Interestingly, when comparing the two cases in which the restrictions on the EMS are extreme ($i_{\min}=0.2$ A/cm² or $|di/dt|_{\max}=0.001$ A/cm²s) the H₂ consumption increases similarly by 6.6%-6.7% with respect to the non-constrained case. This value for the H₂ consumption increase could be considered as the maximum penalty for the best-case control strategy when extreme constraints are imposed on it and it becomes unable to fulfill the charge-sustaining condition in high-dynamics driving conditions.

From these results, it is possible to conclude that even a low limitation in the minimum current density provides a significant decrease in degradation rates at the expense of a small penalty on H₂ consumption. Nonetheless, imposing limits on i_{\min} narrows the operation space of the FC system, thus hindering the fulfillment of the charge-sustaining condition.

5. Simultaneous limitation of $|di/dt|$ and i_{\min}

The effect of limiting $|di/dt|$ and i_{\min} on performance and degradation has been analyzed in sections 3 and 4, respectively. As discussed, the consequences of imposing individually each restriction on the control strategy are similar but caused by different behavior on the current density evolution along the driving cycle. Load-change degradation was the most affected degradation rate source since the imposed constraints had an effect on the FC system dynamics ($|di/dt|$) or in the load-change oscillation amplitude (i_{\min}). In this section, the

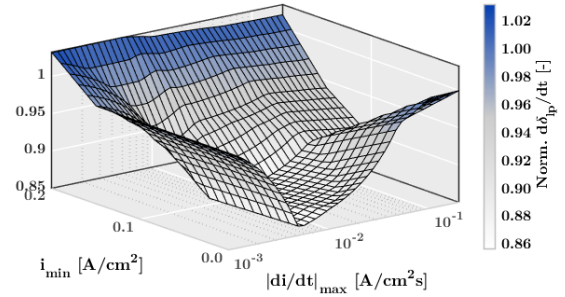


Figure 18: Normalized low-power degradation rate variation with $|di/dt|_{\max}$ and i_{\min} .

cross-effect of both restrictions on the control strategy is investigated to understand whether it is better to impose only one of these limitations or a combination of both to maximize durability and minimize consumption.

Low-power degradation is found to be both dominated by imposing constraints on the dynamics of the FC system ($|di/dt|$) and on the minimum current density since in both cases the overall current density increases, thus minimizing the degradation rate due to high-voltage operation. Figure 18 shows how the trends in figures 7 and 13 remain noticeable except for the cases where extreme limitations are imposed. As a consequence, the minimum low-power degradation rate is found at $|di/dt|_{\max}=0.01$ A/cm²s and $i_{\min}=0.1$ A/cm², i.e., coinciding with the minimums found in figures 7 and 13. This means that the optimal combination of both restrictions on the control strategy may foster the further minimization of the low-power degradation. Nonetheless, when extreme limits are imposed ($|di/dt|_{\max}=0.001$ A/cm²s or $i_{\min}=0.2$ A/cm²) the low-power degradation rate becomes maximum and almost insensitive to any other restriction. This, again, strengthens the argument for avoiding high restrictions in the EMS.

Similar to low-power degradation, medium-power degradation rate also preserves the individual trends when imposing limitations on the dynamics or on the lower limit of the operation space except for extreme constraints (figure 19). In this case, medium-power degradation becomes minimum when $|di/dt|_{\max}=0.001$ A/cm²s or $i_{\min}=0.2$ A/cm² and is almost unaffected when keeping any of these constraints and lowering the other restriction.

As expected, load-change degradation is more affected when limiting the dynamics than when imposing restrictions on the minimum current density (figure 20). Nonetheless, its minimum value is always achieved at

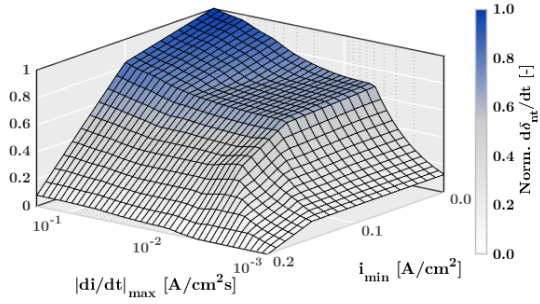


Figure 19: Normalized natural (medium-power) degradation rate variation with $|di/dt|_{\max}$ and i_{\min} .

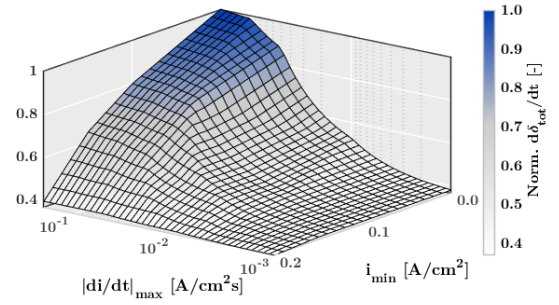


Figure 21: Normalized total degradation rate variation with $|di/dt|_{\max}$ and i_{\min} .

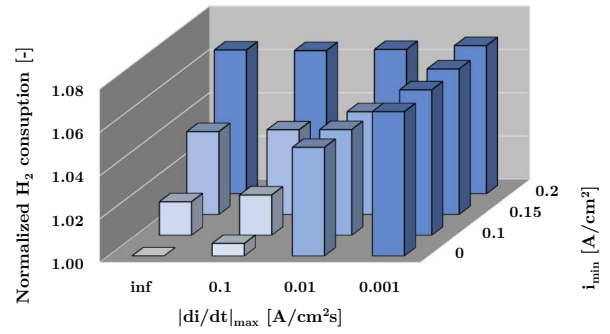


Figure 22: Normalized H_2 consumption variation with $|di/dt|_{\max}$ and i_{\min} .

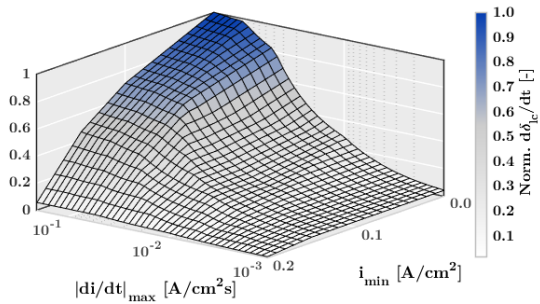


Figure 20: Normalized load-change degradation rate variation with $|di/dt|_{\max}$ and i_{\min} .

extreme limitations, no matter if they are in the dynamics or in the operation space. Load-change degradation rate dominates the total degradation rate, given the similarity of figures 20 and 21, albeit the latter is higher at each restriction due to the addition of the other degradation rates. This is indicative of the fact that even knowing that there are other degradation rate sources that may vary with constraints imposed on the control strategy, load-change degradation dominates the FC stack durability even when alternative restrictions oriented to minimizing other degradation sources (such as limiting i_{\min}) are imposed. Nonetheless, it is imperative to quantify the contribution of the rest of the degradation sources to total degradation since they may become more significant as the EMS is more constrained (figures 10 and 16). This implies that any analysis considering only load-change degradation as the only degradation source that evaluates the change in FC stack durability through changes in the control strategy may definitely overestimate the increase in FC stack durability.

H_2 consumption suffers a similar increase when imposing any limitation, whether it be in the dynamics or in the operation space (figure 22). The max-

imum increase in H_2 with the control strategies considered appears when extreme limitations are imposed ($|di/dt|_{\max}=0.001 \text{ A/cm}^2\text{s}$ or $i_{\min}=0.2 \text{ A/cm}^2$) and is around 6.6-6.7% with respect to the non-limited case. Furthermore, only small constraints in the operation space ($i_{\min}=0.1 \text{ A/cm}^2$) imply 1.5% higher H_2 consumption and 20% lower degradation rate, i.e., 25% higher durability. The reason for this small increase in H_2 consumption is that, even though the limitation prevents the FC system from operating at a very low load where the fuel consumption is low, this operation region usually implies low efficiency since the auxiliary components integrated into the balance of plant have significant consumption compared to the power produced by the FC stack at such a low load.

Interestingly, once the limitation in the dynamics achieves a value of $0.01 \text{ A/cm}^2\text{s}$ or the minimum current density is limited to 0.15 A/cm^2 , the H_2 consumption remains between 3.8% and 5% higher than the non-limited case, except when any of the two constraints is increased. Among these strategies, that with $|di/dt|_{\max}=0.01 \text{ A/cm}^2\text{s}$ and $i_{\min}=0.15 \text{ A/cm}^2$ offers the highest decrease in degradation rate (53%), thus the highest increase in durability (110%) with an increase in H_2 consumption of 4.7%. In this case, it is possible to perceive a cross-effect between the two constraints since a small decrease in H_2 consumption was detected when limiting the dynamics to a fixed value of $0.01 \text{ A/cm}^2\text{s}$ and increasing the i_{\min} . This decrease in H_2 consumption was due to the fact that the dynamic limitation does not allow the FC stack to operate under high loads when the e-motor suffers a sudden increase in the requested load if the FC stack is operating under low current densities. However, if the FC stack operates at higher current densities in the low load region because the i_{\min} is limited, then the FC system power supply will achieve higher loads under sudden increases in the e-motor power demand. This allows the FC system to follow better e-motor operation in the high current density region where the battery needs to provide additional power when the FC system is not capable. As a consequence, if the battery is less discharged, the FC system will not have to provide additional power to fulfill the charge-sustaining mode, thus reducing the H_2 consumption.

5.1. Identification of the optimum control strategy

From the results obtained in previous section, the control strategy with $|di/dt|_{\max}=0.01 \text{ A/cm}^2\text{s}$ and $i_{\min}=0.15 \text{ A/cm}^2$ offered the highest increase in durability (110%) with an increase in H_2 consumption of 4.7%. As such, this design could be considered *recommended*

for this application and vehicle architecture by the authors for the following reasons:

- The dynamics are high enough to fulfill the constant SOC constraint that is characteristic of FCREx architecture even under high-load and high-dynamics driving cycles.
- Minimum current density is high enough to minimize the effect of the degradation mechanisms that appear during high-voltage operation and seems to provide a decrease in H_2 consumption due to a cross effect with the limitations of the dynamic.
- The increase in H_2 consumption is moderate and below 5% in exchange for a significant increase in FC durability.

Nonetheless, it is important to note that this study was performed for a specific application and driving cycle conditions. As such, if the vehicle architecture, dimensions or application change, the optimum constraints in the EMS may also change. For example, if the FCS is integrated into other applications such as forklift captive fleets in which the power demand to the propulsion system is lower and the dynamics are not critical, then the optimum EMS may comprise a set of hybrid operation modes: extremely low dynamics ($|di/dt|_{\max}=0.001 \text{ A/cm}^2\text{s}$) to move the vehicle and allowed high-dynamics during short periods for cargo-lifting. In this sense, changing the driving conditions and the driver profile will undoubtedly affect the FC stack degradation and performance. As such, any EMS implemented for real driving in a real application should consider self-adaptation to the most usual driving profiles it is used for, so the optimum constraints may change. With these considerations, this study serves as a baseline to further develop advanced EMS aiming at optimizing durability and H_2 consumption based on the trends identified from these results.

6. Recommendations for industrial applications

The conclusions from these results bring light to the use of restrictions in the control strategies for FCREx vehicles. As can be perceived in figure 22, any limitation in the EMS implies an increase in H_2 consumption. Hence, the recommendation that can be extracted from these results is that the EMS should be limited in such a way that the FC stack achieves a target value of durability, without over-constraining the EMS to minimize consumption. Furthermore, it may be beneficial to impose limitations on the minimum current density if the

dynamics are limited to a value close to $0.01 \text{ A/cm}^2\text{s}$ since both durability and performance increase. This implies that FCREx manufacturers should consider further limitations in the control strategy of their vehicles apart from imposing slower dynamics in the FC system. In terms of control, given the highly-dynamic behavior that the FC system shows when the dynamics are limited to $0.1 \text{ A/cm}^2\text{s}$, it is recommended for both conventional FCVs and FCREx vehicles to impose at least this limitation in the dynamics to minimize the potential appearance of anode or cathode starvation that may boost degradation. Finally, given a FC stack technology with certain durability, the FCREx manufacturers could estimate the increase in H_2 consumption and durability when imposing different control strategies in such a way that they could minimize the OPEX and the degradation rate simultaneously. The change in the degradation rate can be done independently for each degradation source, hence the durability can be estimated for each FC stack technology.

FC stack or FC systems manufacturers could also use these results when in partnership with OEMs if they intend to manufacture FCREx vehicles. If the OEM considers the use of a certain control strategy with a given set of limitations in the dynamics or in the minimum current density based on these results, the FC stack manufacturers could target a stack design that improves the water and flow management at lower-dynamics conditions or that decreases the high-voltage degradation (low-power) to save costs, maximize performance and durability. Analogously, FC system manufacturers could adjust the balance of plant design in such a way that the requirements in terms of the dynamics for the cathode and/or anode humidification or for the compressor are lower, thus minimizing the manufacturing costs of the powertrain.

7. Conclusion

In this study, the effect on performance and durability of FCREx vehicles when imposing limitations in the dynamics and the minimum current density of the FC system was evaluated. For that purpose, a validated FC stack model was integrated into a FCREx vehicle model together with a real-time energy management strategy optimizer and a semi-empirical PEMFC degradation model. The resulting modeling platform was used to simulate WLTC 3b driving cycles while imposing limitations on the control strategy of the FC system. The limitations affected its dynamics and the minimum current density at which the FC stack can operate, thus having a noticeable effect both on performance

and durability. Differently from other studies, the aim of these simulations was to quantify and detect trends in the H_2 consumption and degradation rates by source evolution when acting over the operational limits of the FC system.

Whether the imposed limitation was on the dynamics or on the minimum current density, it was detected that the most relevant degradation source affected by the limitations in the control strategy was load-change, be it due to the lower intensity in the load-change oscillations or their lower amplitude. Both constraining strategies, when applied individually, were effective to improve the FC stack durability. However, extreme limitations in terms of both dynamics and minimum current density ($|di/dt|_{\max}=0.001 \text{ A/cm}^2\text{s}$ or $i_{\min}=0.2 \text{ A/cm}^2$) were deemed unpractical since, although they increased significantly the durability, they also implied 6.6-6.7% additional H_2 consumption and could potentially prevent the charge-sustaining mode from being fulfilled in high-dynamics driving cycles. When only limiting the dynamics, the cases on which the current density variation rate was limited to 0.01 and $0.001 \text{ A/cm}^2\text{s}$ implied an increase in FC durability to 89% and 166% with a penalty in H_2 consumption of 5% and 6.7%, respectively. This was due to the suboptimum operation in terms of system efficiency due to a much lower load-change intensity and amplitude. Analogously, limiting only i_{\min} to the extreme value of 0.2 A/cm^2 implied a decrease in the degradation of 60% with an increase in H_2 consumption of 6.6-6.7% at the expense of not being able to fulfill the constant SOC condition at some driving cycle conditions, as it happened with the dynamic limitation of $0.001 \text{ A/cm}^2\text{s}$. As such, a maximum dynamic limitation of $|di/dt|_{\max}=0.01 \text{ A/cm}^2\text{s}$ was recommended. For this particular limitation, a cross-effect between control strategies was detected, since imposing limits in the minimum current density when the dynamics is already limited may improve H_2 consumption and durability. The optimum constraints combination that maximizes FC stack lifetime without affecting the vehicle operability was identified to be $|di/dt|_{\max}=0.01 \text{ A/cm}^2\text{s}$ and $i_{\min}=0.15 \text{ A/cm}^2$ since it offers the highest decrease in degradation rate (53%), thus the highest increase in durability (110%) with an increase in H_2 consumption of 4.7%.

Given the significant increase in H_2 consumption when imposing limitations in the control strategy, the authors recommend considering the restrictions in the control strategy that ensures a target life, set by the vehicle manufacturer or the normative, without over-constricting it. As a reference, FCREx vehicles should start with EMS limiting the dynamics and

the operational space to $|di/dt|_{\max}=0.01$ A/cm²s and $i_{\min}=0.15$ A/cm² and further optimize the H₂ and durability, according to the particular targets for the design by refining the value of these limits.

Finally, a set of recommendations for manufacturers of FC stack, FC systems and FCREx vehicles were provided. In this line, the use of these results could speed up the design process of FCREx vehicles by understanding the effect of imposing different control strategies on performance and degradation. FC stack and FC systems manufacturers could also decrease the costs of the inner stack design and balance of plant components through custom design if the OEM purchasing the different components can provide an estimation of the dynamics that the systems are expected to be subjected to. This could help to further increase the efficiency of the overall FCREx vehicle and to provide an estimation of the OPEX variation of FCREx vehicles when imposing different constraints in the FC system control strategy.

Acknowledgments

This research has been partially funded by the Spanish Ministry of Science, Innovation, and University through the University Faculty Training (FPU) program (FPU19/00550) and FEDER and the Generalitat Valenciana, Conselleria d'Innovació, Universitats, Ciència i Societat Digital through project IDIFEDER/2021/039.

References

- [1] Fuel Cells Hydrogen (FCH), Hydrogen Roadmap Europe - a Sustainable Pathway for the European Energy Transition, 1st Edition, Publications Office of the European Union, 2019. doi:10.2843/341510.
- [2] J. M. Desantes, S. Molina, R. Novella, M. Lopez-Juarez, Comparative global warming impact and NOX emissions of conventional and hydrogen automotive propulsion systems, *Energy Conversion and Management* 221 (X) (2020) 113137. doi:10.1016/j.enconman.2020.113137.
- [3] T. Teng, X. Zhang, H. Dong, Q. Xue, A comprehensive review of energy management optimization strategies for fuel cell passenger vehicle, *International Journal of Hydrogen Energy* (xxxx) (2020). doi:10.1016/j.ijhydene.2019.12.202.
- [4] F. Piraino, P. Fragiaco, A multi-method control strategy for numerically testing a fuel cell-battery-supercapacitor tramway, *Energy Conversion and Management* 225 (October) (2020) 113481. doi:10.1016/j.enconman.2020.113481.
- [5] H. Li, A. Ravey, A. N'Diaye, A. Djerdir, Online adaptive equivalent consumption minimization strategy for fuel cell hybrid electric vehicle considering power sources degradation, *Energy Conversion and Management* 192 (March) (2019) 133–149. doi:10.1016/j.enconman.2019.03.090.
- [6] McKinsey, A portfolio of power-trains for Europe: a fact-based analysis - The role of Battery Electric Vehicles, Plug-in Hybrids and Fuel Cell Electric Vehicles, Tech. rep. (2020).
- [7] International Energy Agency, The Future of Hydrogen, Tech. Rep. June (2019). doi:10.1787/1e0514c4-en.
- [8] S. Molina, R. Novella, B. Pla, M. Lopez-Juarez, Optimization and sizing of a fuel cell range extender vehicle for passenger car applications in driving cycle conditions, *Applied Energy* 285 (December 2020) (2021) 116469. doi:10.1016/j.apenergy.2021.116469.
- [9] J. M. Desantes, R. Novella, B. Pla, M. Lopez-Juarez, Impact of fuel cell range extender powertrain design on greenhouse gases and NOX emissions in automotive applications, *Applied Energy* 302 (2021) 117526. doi:10.1016/j.apenergy.2021.117526.
- [10] Z. Sun, Y. Wang, Z. Chen, X. Li, Min-max game based energy management strategy for fuel cell/supercapacitor hybrid electric vehicles, *Applied Energy* 267 (January) (2020) 115086. doi:10.1016/j.apenergy.2020.115086.
- [11] J. O. Leader, Y. Yue, M. R. Walluk, T. A. Trabold, Voltage degradation of high-temperature PEM fuel cells operating at 200 C under constant load and start-stop conditions, *International Journal of Hydrogen Energy* (xxxx) (2022). doi:10.1016/j.ijhydene.2022.04.067.
- [12] K. Song, Y. Ding, X. Hu, H. Xu, Y. Wang, J. Cao, Degradation adaptive energy management strategy using fuel cell state-of-health for fuel economy improvement of hybrid electric vehicle, *Applied Energy* 285 (August 2020) (2021) 116413. doi:10.1016/j.apenergy.2020.116413.
- [13] K. Song, X. Wang, F. Li, M. Sorrentino, B. Zheng, Pontryagin's minimum principle-based real-time energy management strategy for fuel cell hybrid electric vehicle considering both fuel economy and power source durability, *Energy* 205 (2020) 118064. doi:10.1016/j.energy.2020.118064.
- [14] P. Pei, Q. Chang, T. Tang, A quick evaluating method for automotive fuel cell lifetime, *International Journal of Hydrogen Energy* 33 (14) (2008) 3829–3836. doi:10.1016/j.ijhydene.2008.04.048.
- [15] S. Quan, Y. X. Wang, X. Xiao, H. He, F. Sun, Real-time energy management for fuel cell electric vehicle using speed prediction-based model predictive control considering performance degradation, *Applied Energy* 304 (August) (2021) 117845. doi:10.1016/j.apenergy.2021.117845.
- [16] F. Peng, Y. Zhao, T. Chen, X. Zhang, W. Chen, D. Zhou, Q. Li, Development of robust suboptimal real-time power sharing strategy for modern fuel cell based hybrid tramways considering operational uncertainties and performance degradation, *Applied Energy* 226 (April) (2018) 503–521. doi:10.1016/j.apenergy.2018.05.092.
- [17] Y. He, Y. Zhou, Z. Wang, J. Liu, Z. Liu, G. Zhang, Quantification on fuel cell degradation and techno-economic analysis of a hydrogen-based grid-interactive residential energy sharing network with fuel-cell-powered vehicles, *Applied Energy* 303 (August) (2021) 117444. doi:10.1016/j.apenergy.2021.117444.
- [18] Y. Wang, S. J. Moura, S. G. Advani, A. K. Prasad, Power management system for a fuel cell/battery hybrid vehicle incorporating fuel cell and battery degradation, *International Journal of Hydrogen Energy* 44 (16) (2019) 8479–8492. doi:10.1016/j.ijhydene.2019.02.003.
- [19] Y. Wang, S. G. Advani, A. K. Prasad, A comparison of rule-based and model predictive controller-based power management strategies for fuel cell/battery hybrid vehicles considering degradation, *International Journal of Hydrogen Energy* 45 (58) (2020) 33948–33956. doi:10.1016/j.ijhydene.2020.09.030.
- [20] Y. Zhou, A. Ravey, M. C. Péra, Multi-mode predictive energy management for fuel cell hybrid electric vehicles using Markov driving pattern recognizer, *Applied Energy* 258 (October 2019) (2020) 114057. doi:10.1016/j.apenergy.2019.114057.
- [21] X. Lin, X. Xu, H. Lin, Predictive-ECMS based degradation pro-

- protective control strategy for a fuel cell hybrid electric vehicle considering uphill condition, *eTransportation* 12 (2022) 100168. doi:10.1016/j.etrans.2022.100168.
- [22] L. Xing, W. Xiang, R. Zhu, Z. Tu, Modeling and thermal management of proton exchange membrane fuel cell for fuel cell/battery hybrid automotive vehicle, *International Journal of Hydrogen Energy* 47 (3) (2022) 1888–1900. doi:10.1016/j.ijhydene.2021.10.146.
- [23] Y. Zhou, H. Obeid, S. Laghrouche, M. Hilairret, A. Djerdir, A novel second-order sliding mode control of hybrid fuel cell/super capacitors power system considering the degradation of the fuel cell, *Energy Conversion and Management* 229 (September 2020) (2021) 113766. doi:10.1016/j.enconman.2020.113766.
- [24] R. Ma, T. Yang, E. Breaz, Z. Li, P. Briois, F. Gao, Data-driven proton exchange membrane fuel cell degradation prediction through deep learning method, *Applied Energy* 231 (July) (2018) 102–115. doi:10.1016/j.apenergy.2018.09.111.
- [25] M. Ou, R. Zhang, Z. Shao, B. Li, D. Yang, P. Ming, C. Zhang, A novel approach based on semi-empirical model for degradation prediction of fuel cells, *Journal of Power Sources* 488 (December 2020) (2021) 229435. doi:10.1016/j.jpowsour.2020.229435.
- [26] M. Raeesi, S. Changizian, P. Ahmadi, A. Khoshnevisan, Performance analysis of a degraded PEM fuel cell stack for hydrogen passenger vehicles based on machine learning algorithms in real driving conditions, *Energy Conversion and Management* 248 (2021) 114793. doi:10.1016/j.enconman.2021.114793.
- [27] Y. Zhou, H. Li, A. Ravey, M. C. Péra, An integrated predictive energy management for light-duty range-extended plug-in fuel cell electric vehicle, *Journal of Power Sources* 451 (January) (2020). doi:10.1016/j.jpowsour.2020.227780.
- [28] H. Zhang, X. Li, X. Liu, J. Yan, Enhancing fuel cell durability for fuel cell plug-in hybrid electric vehicles through strategic power management, *Applied Energy* 241 (January) (2019) 483–490. doi:10.1016/j.apenergy.2019.02.040.
- [29] F. Martel, Y. Dubé, S. Kelouwani, J. Jagemont, K. Agbossou, Long-term assessment of economic plug-in hybrid electric vehicle battery lifetime degradation management through near optimal fuel cell load sharing, *Journal of Power Sources* 318 (2016) 270–282. doi:10.1016/j.jpowsour.2016.04.029.
- [30] K. Chen, S. Laghrouche, A. Djerdir, Degradation model of proton exchange membrane fuel cell based on a novel hybrid method, *Applied Energy* 252 (May) (2019) 113439. doi:10.1016/j.apenergy.2019.113439.
- [31] I. Terada, H. Nakagawa, *Polymer Electrolyte Fuel Cell*, *Kobunshi* 57 (7) (2008) 498–501. doi:10.1295/kobunshi.57.498.
- [32] D. Murschenhofer, D. Kuzdas, S. Braun, S. Jakubek, A real-time capable quasi-2D proton exchange membrane fuel cell model, *Energy Conversion and Management* 162 (January) (2018) 159–175. doi:10.1016/j.enconman.2018.02.028.
- [33] P. Corbo, F. Migliardini, O. Veneri, Experimental analysis and management issues of a hydrogen fuel cell system for stationary and mobile application, *Energy Conversion and Management* 48 (8) (2007) 2365–2374. doi:10.1016/j.enconman.2007.03.009.
- [34] P. Corbo, F. Migliardini, O. Veneri, Experimental analysis of a 20 kWe PEM fuel cell system in dynamic conditions representative of automotive applications, *Energy Conversion and Management* 49 (10) (2008) 2688–2697. doi:10.1016/j.enconman.2008.04.001.
- [35] J. M. Desantes, R. Novella, B. Pla, M. Lopez-Juarez, A modeling framework for predicting the effect of the operating conditions and component sizing on fuel cell degradation and performance for automotive applications, *Applied Energy* 317 (November 2021) (2022) 119137. doi:10.1016/j.apenergy.2022.119137.
- [36] S. Knights, *Polymer Electrolyte Membrane and Direct Methanol Fuel Cell Technology: 6 - Operation and durability of low temperature fuel cells*, Woodhead Publishing Limited, 2012. doi:10.1533/9780857095473.2.137.
- [37] K. H. Kangasniemi, D. A. Condit, T. D. Jarvi, Characterization of Vulcan Electrochemically Oxidized under Simulated PEM Fuel Cell Conditions, *Journal of The Electrochemical Society* 151 (4) (2004) E125. doi:10.1149/1.1649756.
- [38] W. Bi, T. F. Fuller, Temperature Effects on PEM Fuel Cells PtC Catalyst Degradation, *Journal of The Electrochemical Society* 155 (2) (2008) B215. doi:10.1149/1.2819680.
- [39] M. Dutta, N. Jia, S. Lu, V. Colbow, S. Wessel, Effects of Upper Potential Dwell Time, Transients and Relative Humidity on PEM Fuel Cell Cathode Catalyst Degradation, *The Electrochemical Society 217th Meeting (c)* (2010).
- [40] S. Onori, L. Serrao, G. Rizzoni, *Hybrid electric vehicles: Energy management strategies*, Springer, 2016.
- [41] L. Serrao, S. Onori, G. Rizzoni, Ecms as a realization of ponytryagin's minimum principle for hev control, in: 2009 American control conference, IEEE, 2009, pp. 3964–3969.